

DYNAMICS OF BEC MIXTURES LOADED INTO THE OPTICAL LATTICE IN THE PRESENCE OF LINEAR INTER-COMPONENT COUPLING

M.Yu. Uleysky¹, D.V. Makarov^{1*}

¹ *V.I. Il'ichev Pacific Oceanological Institute of FEB RAS
Vladivostok, Russia*

*Corresponding author e-mail: makarov @ poi.dvo.ru

Abstract

We consider dynamics of a two-component Bose-Einstein condensate where the components correspond to different hyperfine states of the same sort of atoms. External microwave radiation leads to resonant transitions between the states. The condensate is loaded into the optical lattice. We invoke the tight-binding approximation and examine the interplay of spatial and internal dynamics of the mixture. It is shown that internal dynamics qualitatively depends on the intra-component interaction strength and the phase configuration of the initial state. We focus attention on two intriguing phenomena occurring for certain parameter values. The first phenomenon is the spontaneous synchronization of Rabi oscillations running inside neighbouring lattice sites. Another one is the demixing of the condensate with formation of immiscible solitons when nonlinearity becomes sufficiently strong. Demixing is preceded by the transient regime with highly irregular behavior of the mixture.

Keywords: Bose-Einstein condensate, optical lattice, Rabi transitions, synchronization, solitons.

1 Introduction

Two-component Bose-Einstein condensates with linear inter-component coupling have become an object of considerable interest associated with their non-trivial dynamical properties, such as onset of self-trapping in Rabi oscillations, π -oscillations [1], bifurcations in Rabi oscillations [2], miscibility-immiscibility transitions induced by Rabi coupling [3, 4], to name a few. Owing to the close analogy with Josephson transitions, these two-component mixtures are often referred to as the Bose-Josephson junctions [1, 5]. They are also considered as advantageous tools for storage of quantum information [6], or for manufacturing of high-precision atomic clocks [7].

Usually, two ways of composing a Bose-Josephson junction are considered. The first one is based on the creation of the double-well optical potential. Then different components relate to the condensate fractions trapped inside different wells, and the linear inter-component coupling is provided by inter-well tunneling. The second way is the usage of condensates occupying the same trap but belonging to different hyperfine energy levels. The resonant microwave radiation causes transitions between the levels, providing linear inter-component coupling. In both these situations atomic ensembles are tightly

confined inside the optical trap, and spatial expansion of the condensate is limited. Elimination of the BEC expansion allows one to describe the inter-component transitions by means of the classical equations of motion corresponding to a pendulum-like Hamiltonian [1, 2]. Meanwhile, it is reasonable to examine the case when the mixture of two linearly-coupled hyperfine states is loaded into the optical lattice and allowed to expand along many potential wells, that is, spatial BEC expansion cannot be eliminated. This system can be regarded as an array of Bose-Josephson junctions [8] and considered as a promising way for creating large-scale entangled states [9, 10]. However, it is well known that interplay between external (i.e. spatial) and internal (corresponding to level transitions) degrees of freedom can essentially complexify atom dynamics even in the absence of interactions between atoms. Earlier studies in the semiclassical regime for the spatial atomic dynamics revealed many intriguing phenomena like chaotic Rabi oscillations [11], chaotic atomic transport and dynamical fractals [12–15], occurrence of Lévy flights and anomalous diffusion [16–18], synchronization between spatial and internal dynamics [19]. A detailed theory of chaotic atomic transport of atoms in a laser standing wave has been developed in Refs. [15, 20, 21]. Obviously, presence of interactions between atoms should cause additional complications of the underlying physics.

In the present work we consider the BEC mixture loaded into the lattice in the presence of interactions between atoms. Our main goal is to describe the main regimes of spatial and internal dynamics of the BEC mixture, and to study how dynamics of Rabi oscillations changes with increasing the interaction strength. The paper is organized as follows. In the next section we represent the model considered and give brief description of the dynamics when tunneling between neighbouring lattice sites is negligible and there is no spatial condensate expansion. Section 3 describes spatial BEC dynamics when tunneling becomes significant. In section 4 we examine how spatial dynamics influences inter-component transitions. The results obtained are discussed in Summary.

2 General theory

2.1 Basic equations

Within the mean-field approximation, the condensate dynamics is governed by the coupled Gross-Pitaevskii equations

$$\begin{aligned} i\hbar\frac{\partial\Psi_1}{\partial t} &= -\frac{\hbar^2}{2m}\frac{\partial^2\Psi_1}{\partial x^2} + U(x)\Psi_1 + g_1|\Psi_1|^2\Psi_1 + g_{12}|\Psi_2|^2\Psi_1 - \frac{\hbar\Omega}{2}\Psi_2, \\ i\hbar\frac{\partial\Psi_2}{\partial t} &= -\frac{\hbar^2}{2m}\frac{\partial^2\Psi_2}{\partial x^2} + U(x)\Psi_2 + g_2|\Psi_2|^2\Psi_2 + g_{12}|\Psi_1|^2\Psi_2 - \frac{\hbar\Omega}{2}\Psi_1 + \delta\Psi_2, \end{aligned} \quad (1)$$

where Ψ_1 and Ψ_2 are macroscopic wave functions corresponding to the first and the second hyperfine states, respectively, $U(x)$ is the lattice potential, g_1 and g_2 are the nonlinearity parameters corresponding to intra-component interaction, g_{12} is the nonlinearity parameter quantifying the inter-component interaction, Ω is the Rabi frequency being the rate of the inter-component transitions, and δ is the transition detuning. Hereafter we shall consider the case of $\delta = 0$.

In the absence of Rabi coupling, $\Omega = 0$, spatial dynamics is controlled by the lattice height and nonlinearity parameters. The lattice height determines the rate of tunneling between neighbouring sites. Strong nonlinearity can significantly reduce the wavepacket expansion due to spatial self-trapping [22,

23]. In addition, dynamics of two-component condensate mixtures with repulsive interactions (positive nonlinearity parameters) between atoms qualitatively depends on whether this mixture is miscible or not. The condition of immiscibility can be formulated as follows

$$g_{12}^2 > g_1 g_2, \quad (2)$$

i. e. inter-component repulsion should prevail over intra-component repulsion. Presence of the Rabi coupling can drive the mixture from miscible to immiscible regime and vice versa [3,4]. In experiments, each of the nonlinearity parameters g_1 , g_2 and g_{12} can be tuned via the Feshbach resonance. As long as different components correspond to the same atoms, one can assume $g_1 = g_2 \equiv g$.

If the lattice is sufficiently deep, one can simplify the problem by means of the tight-binding approximation [24–26]. In this way, it is assumed that the majority of energy is preserved in the first energy band, and one can expand the wavefunctions Ψ_1 and Ψ_2 over first-band Wannier states corresponding to the decoupled problem, i. e. $\Omega = 0$. One has to take care that the tight-binding approximation becomes essentially questionable if the criterion (2) is satisfied. In the immiscible regime, initially uniform mixture undergoes fragmentation due to spatial separation of different components inside individual lattice sites [27,28], that is, the wavepackets occupying individual lattice sites acquire essentially non-symmetric form and cannot be represented as superposition of the first-band Wannier states. Taking this into account, we set $g_{12} = 0$ inferring the most unfavorable conditions for demixing. Thus, Eqs. (1) reduce to the coupled discrete Gross-Pitaevskii equations

$$\begin{aligned} i\hbar \frac{da_n}{dt} &= -J(a_{n-1} + a_{n+1}) + g|a_n|^2 a_n - \frac{\hbar\Omega}{2} b_n, \\ i\hbar \frac{db_n}{dt} &= -J(b_{n-1} + b_{n+1}) + g|b_n|^2 b_n - \frac{\hbar\Omega}{2} a_n, \end{aligned} \quad (3)$$

where a_n and b_n are complex-valued amplitudes of the condensate wave function at the lattice site n , J is the hopping rate describing tunneling between neighbouring sites. To our knowledge, the first systematic study of such models was presented in [29], where some particular analytical solutions were found. Similar models were considered in [30,31]. Hereafter we shall use the scaling of variables which corresponds to $\hbar = 1$.

2.2 Uncoupled lattice sites

Firstly, let's consider the case of uncoupled lattice sites, $J = 0$. It corresponds to large values of the lattice potential height, when tunneling can be neglected. In this case total occupation of each site

$$\rho_n = |a_n|^2 + |b_n|^2 \quad (4)$$

is time-independent. Substituting

$$a = |a_n| e^{i\alpha_n}, \quad b = |b_n| e^{i\beta_n} \quad (5)$$

into (3), and after some simple algebra, we obtain the system of equations

$$\begin{aligned} \dot{z}_n &= \sqrt{1 - z_n^2} \sin \phi_n, \\ \dot{\phi}_n &= \Lambda_n z_n + \frac{z_n}{\sqrt{1 - z_n^2}} \cos \phi_n, \end{aligned} \quad (6)$$

where the dot denotes differentiation with respect to the rescaled time $t' = \Omega t$,

$$z_n = \frac{|a_n|^2 - |b_n|^2}{\rho_n} \quad (7)$$

is the normalized population imbalance corresponding to the n -th lattice site,

$$\phi_n = \arg a_n b_n^* \equiv \alpha_n - \beta_n, \quad (8)$$

$\Lambda_n = g\rho_n/(\hbar\Omega)$. Equations (6) originate from the classical Hamiltonian

$$H(z_n, \phi_n) = \frac{\Lambda_n z_n^2}{2} - \sqrt{1 - z_n^2} \cos \phi_n. \quad (9)$$

This expression is similar to the Hamiltonian of the nonlinear pendulum. The main difference is the presence of the factor $(1 - z_n^2)^{1/2}$. As this factor depends on z_n , the phase space structure corresponding to the Hamiltonian (9) crucially depends on the parameter Λ . If $\Lambda_n < 1$, i. e. in the case of weak nonlinearity, the phase portrait corresponding to Eqs. (6) contains a family of center fixed points located at $z_n = 0$, $\phi_n = \pi m$, $m = 1, 2$. Any trajectory of (6) is rotation in phase space around one of the fixed points [2]. It corresponds to oscillations of the population imbalance z_n with zero mean. This dynamical regime can be referred to as the Rabi regime [33].

If $\Lambda_n > 1$, the fixed point located at $z_n = 0$, $\phi_n = \pi$ undergoes the pitchfork bifurcation, that is, it transforms into three fixed points, one saddle and two centers. The saddle fixed point is located at $z_n = 0$, $\phi_n = \pi$, i. e. at the same place as the center fixed point before the bifurcation. The “new” center fixed points are located at $z_n = \pm\sqrt{1 - \Lambda_n^{-2}}$, $\phi_n = \pi$. Each of them is surrounded by the domain of population imbalance oscillations with nonzero mean, that is, one component dominates over another. This regime can be referred to as the *internal self-trapping*. This phenomenon was earlier observed for the cases of interacting [2] and non-interacting [34] atoms. Further growth of the interaction strength g moves the center fixed points towards limiting values of the population imbalance, $z_n = \pm 1$, with increasing of the phase space area corresponding to the internal self-trapping.

3 Spatial dynamics of the mixture in the optical lattice

For moderate values of the optical potential height, $U_0 \sim 10$ recoil energies or less, tunneling between lattice sites becomes meaningful and has to be taken into account. Tunneling results in spatial spreading of an atomic wavepacket along the lattice, thereby reducing local condensate density. However, if the interaction energy

$$E_{\text{int}} = g \sum_n (|a_n|^4 + |b_n|^4) \quad (10)$$

exceeds some threshold value, there can occur spatial self-trapping, when wavepacket depletion becomes very slow due to formation of steady soliton-like states [23]. Spatial spreading also depends on the wavepacket form, in particular, on its width and spatial modulation [22, 32]. All the computations presented in this paper were performed with $J = 1$.

In order to study the effect of spatial modulation, let's consider the initial condition of the following form:

$$a_n(t=0) = A \exp\left[-\frac{n^2}{4\sigma^2}\right] \cos \pi p n, \quad b_n = 0, \quad (11)$$

where $p \in [0 : 2]$, $-N \leq n \leq N$, $\sigma = 10$, the factor A is determined by the normalization condition

$$\sum_{n=-N}^N |\psi_n|^2 = 1.$$

Throughout this paper we perform computations for the lattice with 10001 sites, i. e. $N = 5000$. With this normalization, information about number of condensed atoms and s-wave scattering length is hidden in the nonlinearity parameter g . In order to distinguish different regimes of nonlinearity, it is convenient to set a value of the interaction energy E_{int} , and then compute the corresponding value of the nonlinearity parameter by means of the formula

$$g = \frac{E_{\text{int}}}{\sum_{n=-N}^N |a_n(t=0)|^4}. \quad (12)$$

In the absence of Rabi coupling, wavepacket dynamics qualitatively depends on the parameter p which describes phase configuration of the initial state [22, 32]. The case of $p = 0$ corresponds to the same wavepacket phases for all lattice sites, while the case of $p = 1$ means the checkboard-like ordering of phases 0 and π . The case of $p = 0.5$ also means the checkboard sequence, but the sites with phases 0 and π are separated by unoccupied sites. If the wavepacket width is sufficiently large, $\sigma \sim 10$, the strongest spreading is expected in the absence of spatial modulation of the initial state, i. e. for $p = 0$ or $p = 2$, while the strongest spatial self-trapping is anticipated for $p = 0.5$ or $p = 1.5$. The intermediate case of $p = 1$ is the most favorable from the viewpoint of the breather formation [22].

BEC expansion along the lattice can be quantified by position variance

$$\sigma = \sqrt{\sum_n n^2 \rho_n - \left(\sum_n n \rho_n\right)^2}, \quad (13)$$

or by the participation ratio

$$\Gamma = \frac{1}{\sum_n \rho_n^2}, \quad (14)$$

where ρ_n is given by (4). The participation ratio is approximately equal to the number of lattice sites which are efficiently occupied.

Left panel of figure 1 represents the map of participation ratio values computed at $t = 1000\pi$. Coordinates of the map are the parameter p and the interaction energy E_{int} . There is sharp contrast between “dark” regions corresponding to fast condensate depletion due to spatial diffusion, and “light” region where the condensate concentration remains sufficiently high. The light region becomes broader with increasing E_{int} , reflecting onset of spatial self-trapping. It involves notable vertical lines corresponding to $p = 0.5, 1.0$ and 1.5 . The lines at $p = 0.5$ and 1.5 correspond to smaller spreading as compared with the nearest background, while the line at $p = 0$ looks a little more dark and corresponds to larger spreading. These results are qualitatively consistent with theoretical predictions of [22]. To examine the difference

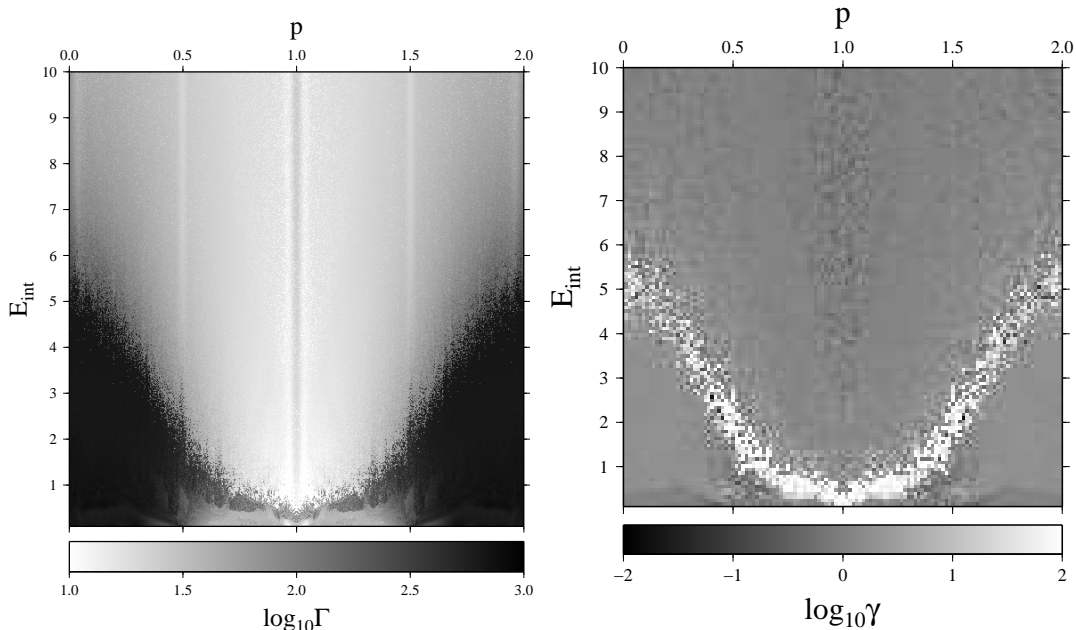


Figure 1: Left: the map of participation ratio values computed at $t = 1000\pi$. Right: the map of relative differences between the participation ratios computed with and without Rabi coupling. Color scales for both plots are presented below.

brought in by the Rabi coupling, it is reasonable to compare the above results with the results obtained without the Rabi coupling. It is made in the right panel of Fig. 1, where we plot the map of the quantity defined as

$$\gamma = \frac{\Gamma(\Omega = 1, t = 1000\pi)}{\Gamma(\Omega = 0, t = 1000\pi)}. \quad (15)$$

If the Rabi coupling results in increasing (decreasing) of condensate spreading, then this quantity is larger (smaller) than 1. The most prominent difference is observed near the boundary separating “dark” and “light” parameter regions in the left panel. Near this boundary, the Rabi coupling slightly extends the parameter area corresponding to fast spatial diffusion. This can be understood as reduction of intra-component interactions due to component interconversion. Indeed, the interaction energy oscillates in the presence of the Rabi coupling, and its time-averaged value becomes smaller. On the other hand, one can see a cloud of dark points in the region corresponding to $p = 0$ and large values of E_{int} . It means that, in the regime of strong nonlinearity, Rabi coupling can weaken the spreading of a wavepacket.

Figures 2 and 3 illustrate the process of wavepacket spreading for different values of the interaction energy. In particular, we shall consider the cases of $E_{\text{int}} = 0.1$ and $E_{\text{int}} = 1$, referring to them as the regime of weak and moderate intra-component interactions, respectively. We consider initial wavepackets with $p = 0, 0.5$ and 1 . Let’s begin with considering Fig. 2 demonstrating time dependence of the position variance. In the regime of weak intra-component interactions, $E_{\text{int}} = 0.1$, the variance grows on the ballistic manner (see Fig. 2a). Notably, rate of the growth for the case of $p = 0.5$ is remarkably larger than for $p = 0$ and $p = 1$. Ballistic expansion is also observed in the case of moderate intra-component interactions, $E_{\text{int}} = 1$, but the difference between different values of p becomes not so apparent (see

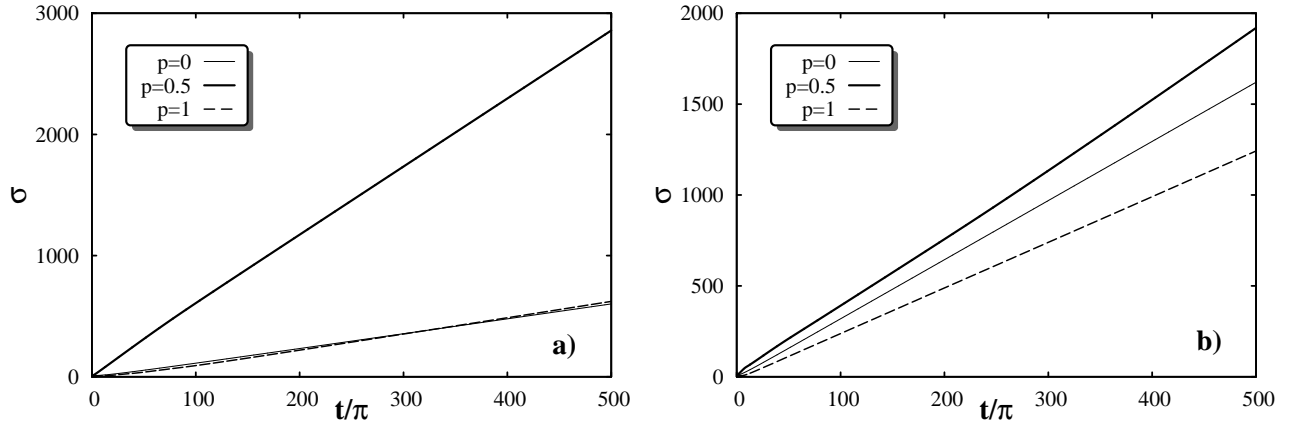


Figure 2: Position variance σ as function of time for different values of the interaction energy: a) $E_{\text{int}} = 0.1$, b) $E_{\text{int}} = 1$. Rabi frequency $\Omega = 1$ for all cases.

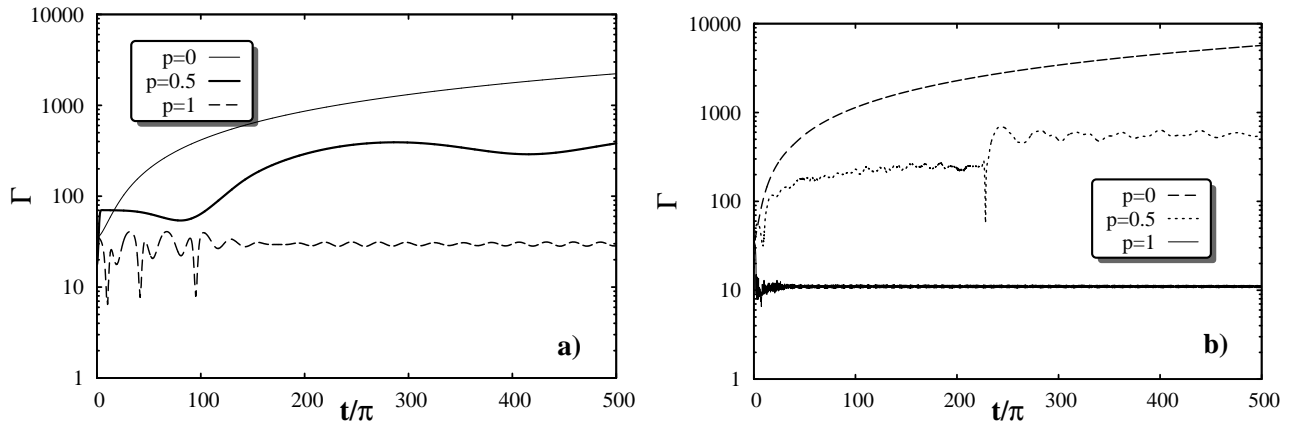


Figure 3: Participation ratio as function of time for different values of the interaction energy: a) $E_{\text{int}} = 0.1$, b) $E_{\text{int}} = 1$. Rabi frequency $\Omega = 1$ for all cases.

Fig. 2b).

Evolution of participation ratio is presented in Fig. 3. One can see that number of sites occupied by the wavepacket with $p = 1$ varies weakly for both regimes of nonlinearity. This can be thought of as a signature of self-trapping and breather formation. The opposite situation is observed in the case $p = 0$, when to the most fastest growth of the participation ratio anticipates the strongest tendency to diffusion. In the case of $p = 0.5$, fast growth of σ in the regimes of weak or moderate intra-component interactions is accompanied by relatively weak growth of the participation number. This indicates on the formation of ballistically moving breathers.

4 Internal dynamics

4.1 Weak intra-component interaction

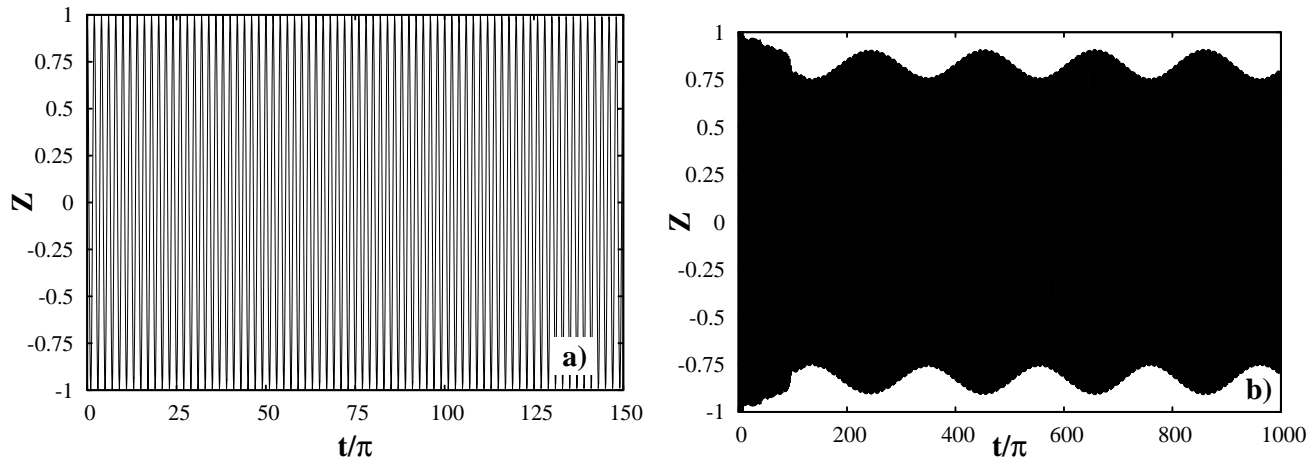


Figure 4: Total population imbalance as function of time for the case of weak intra-component interactions, $E_{\text{int}} = 0.1$. a) $p = 0$, b) $p = 1$.

Let's consider how spatial dynamics of the mixture influences inter-level transitions. For this purpose, it is reasonable to examine evolution of the total population imbalance (TPI)

$$Z = \sum_n \rho_n z_n = \sum_n |a_n|^2 - \sum_n |b_n|^2. \quad (16)$$

Firstly, let's consider the case of weak intra-component interaction. Figure 4 illustrates dependence of TPI on time for $p = 0$ and $p = 1$. In both these cases, TPI undergoes oscillations which are typical for the Rabi regime. In the case of $p = 0$, these oscillations are almost completely coherent and their amplitude is close to the maximal value. It means that linear Rabi coupling provides complete and synchronous component interconversion. The same behavior is observed in the case of the initial state with $p = 0.5$. In the case of $p = 1$ the situation is qualitatively different, and the amplitude of TPI oscillations varies periodically with time, as is demonstrated in Fig. 4b. This difference comes from the difference in spatial behavior. In the case of $p = 0$, spatial wavepacket expansion is accompanied by fast growth of the participation ratio. Therefore, local condensate density rapidly decreases and intra-component interaction becomes negligible. This results in decoupling of translational and internal degrees of freedom, that is, all the lattice sites undergo synchronous Rabi oscillations. In the case of $p = 1$, the condensate depletion is much weaker (see Fig. 3a) due to formation of two distinct pairs of breathers. Each pair consists of identical breathers disposed symmetrically with respect to the center of the initial state. i. e., $n = 0$. Difference in condensate densities of the pairs results in the difference in frequencies of Rabi oscillations, therefore, TPI varies quasiperiodically like sum of two harmonic functions.

4.2 Moderate intra-component interaction

Increasing of nonlinearity in (3) gives rise to anharmonicity in inter-level transitions. Impact of nonlinearity depends on local density of the condensate, therefore, frequencies of Rabi oscillations at different

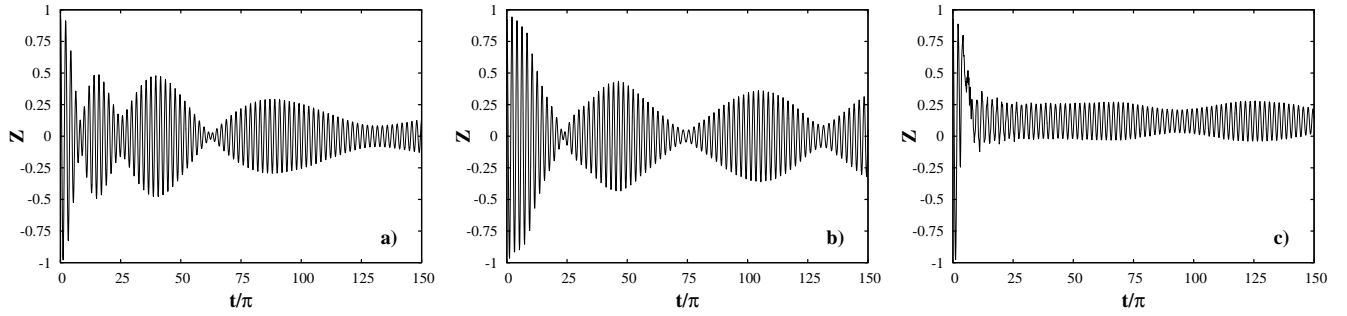


Figure 5: Population imbalance as function of time for the case of moderate intra-component interactions, $E_{\text{int}} = 1$. a) $p = 0$, b) $p = 0.5$, c) $p = 1$.

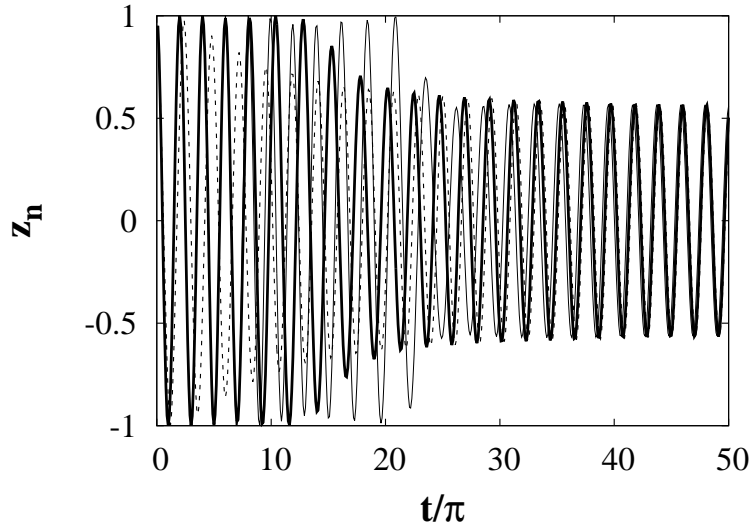


Figure 6: Synchronization of Rabi oscillations corresponding to the sites $n = 0$ (dashes), $n = 30$ (thick solid) and $n = 50$ (thin solid).

lattice sites don't coincide. The frequency offsets destroy the synchronization of Rabi oscillations. As a consequence, the resulting TPI oscillations become the superposition of many independent oscillations running inside individual lattice sites, and the maximal amplitude of TPI oscillations is significantly lower than in the case of weak intra-component interaction.

However, if the intra-component interaction is not very strong, large fraction of the condensate near the center of the initial state can maintain synchronization, giving rise to a large domain with coherent Rabi dynamics. This regime is realized in the case of the initial state with $p = 0$ (see Fig. 5a). As it follows from Fig. 6, there occurs spontaneous synchronization of Rabi oscillations corresponding to different lattice sites. Phase portraits in the $z_n - \phi_n$ plane, constructed for individual lattice sites, are very similar to each other and look as is demonstrated in Fig. 7. The marked common feature is the presence of the limit cycle whose phase space location is nearly the same for all synchronized sites. This

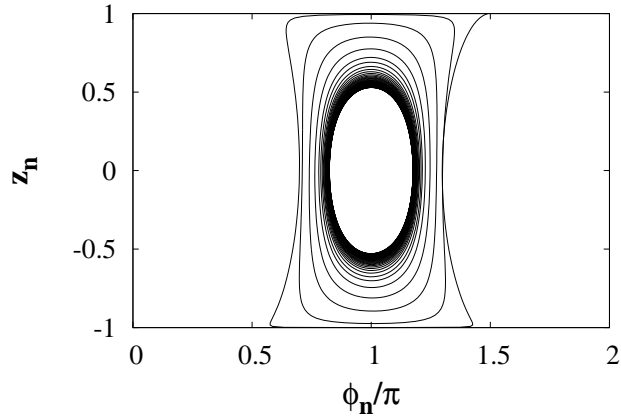


Figure 7: Typical phase portrait describing inter-component transitions inside an individual lattice site for $p = 0$. ϕ_n is given by (8).

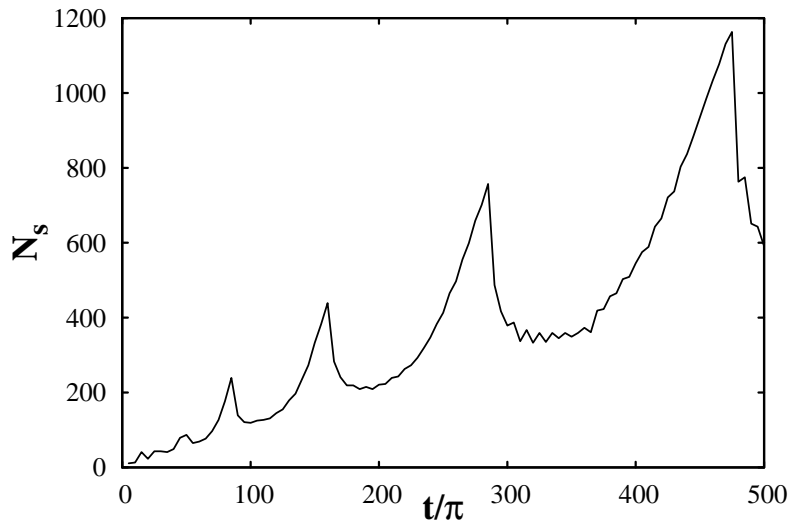


Figure 8: Number of synchronized sites as function of time.

may appear somewhat surprising. Indeed, limit cycles can occur only in the presence of dissipation while the equations (3) don't contain dissipative terms. However, the role of dissipation can be played by one-way energy transfer between degrees of freedom. In our case, energy from the internal degree of freedom, associated with the Rabi coupling, is absorbed by the external degrees of freedom, namely spatial wavepacket motion and intra-component interaction. Hence, there arises synchronization inherent of non-Hamiltonian systems.

Taking into account that the domain of synchronized Rabi oscillations is placed in the center of the lattice, one can define the criterion of synchronization as inequality

$$|z_n(t) - z_{n'}(t)| \leq C, \quad -n' \leq n \leq n'. \quad (17)$$

Here C is some small constant. We set $C = 0.1$ in order to estimate number of synchronized sites

$$N_s = 2n' + 1, \quad (18)$$

Time dependence of N_s is presented in Fig. 8. It is demonstrated that N_s undergoes pulsations with growing amplitude. It implies that some lattice sites can exit the synchronized regime and then return into it. This phenomenon indicates on the presence of wave-like excitations inside the domain of synchronization, reminiscent of magnons. Comparison with Fig. 3b allows one to link the growth of pulsations amplitude with increasing of participation ratio, that is, more and more lattice sites become synchronized as the condensate expands along the lattice.

In the case of the initial state with $p = 0.5$, TPI also undergoes oscillations with decaying amplitude, as is shown in Fig. 5b. However, there is no synchronization, and the amplitude decay is associated with dephasing of Rabi oscillations running at different sites.

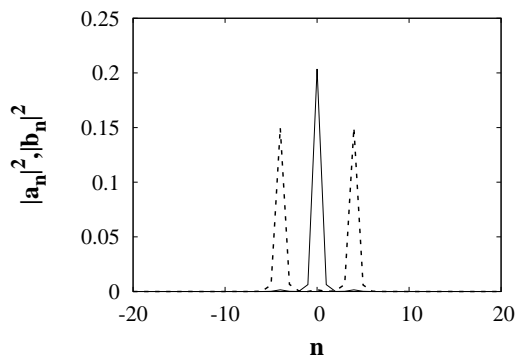


Figure 9: Squared modulo of wavefunctions corresponding to the first (solid) and second (dotted) components at $t = 500\pi$.

Initial state with $p = 1$ behaves in a qualitatively different way as compared with $p = 0$ and $p = 0.5$. As one can see in Fig. 5c, TPI undergoes oscillations with non-zero mean, i. e. the first component of the mixture prevails over the second one. It indicates on the onset of internal self-trapping, the effect discussed in Section 2.2. In the absence of coupling between sites, internal self-trapping is linked to the bifurcation of fixed points according to the scenario described in Section 2.2. However, one should expect that tunneling between neighbouring sites should destroy the phase coherence needed for the onset regular oscillations around displaced fixed points. This means that the onset of the internal self-trapping should occur when tunneling is weak. In this way, it is worth reminding that the initial state with $p = 1$ is characterized by the strongest spatial self-trapping, that is, the tunneling is suppressed due to formation of localized states like breathers or solitons. These localized states are presented in Fig. 9. It should be noted that they are well separated in space, that is, they don't affect each other. This means that inter-component dynamics of every such state can be fairly described within a single-site approximation corresponding to the Eqs. (6). Figure 10 illustrates population imbalance oscillations corresponding to the center (left figure) and right (right figure) localized states depicted in Fig. 9. After short irregular transient regime, population imbalance becomes frozen in both cases, indicating the total dominance of one component. It means that the localized states can be thought of as immiscible solitons. Thus, it turns out that stable internal self-trapping occurs in the presence of spatial self-trapping.

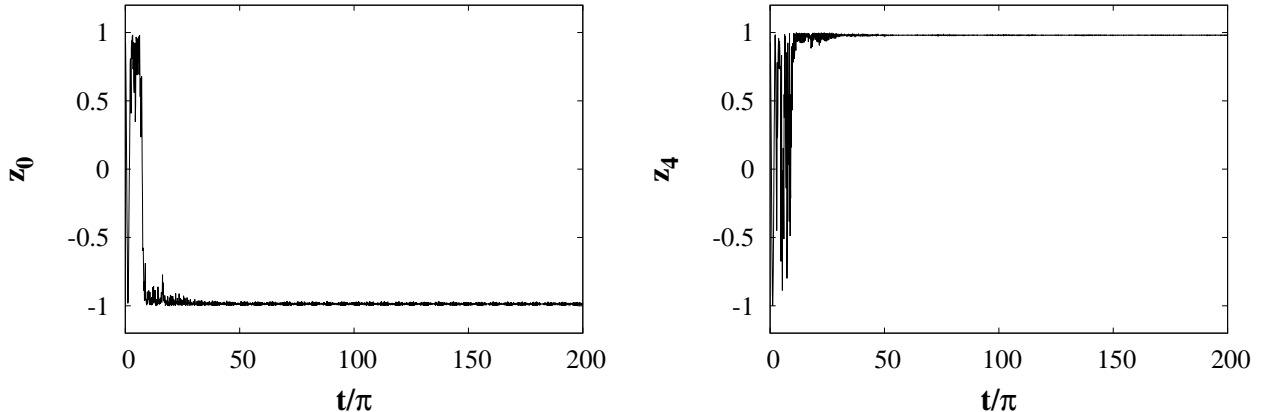


Figure 10: Population imbalances corresponding to the lattice sites $n = 0$ (left figure) and $n = 4$ (right).

5 Summary

The present work is devoted to dynamics of two-component BEC with linear inter-component coupling loaded into the optical lattice. The main goal is to describe the interplay between spatial and internal degrees of freedom. It is found that spatial mixture dynamics is readily controlled by the interaction strength and phase configuration of the initial state, i. e. likewise in the case of one-component condensate [22]. If condensate undergoes fragmentation with occurrence of localized and isolated patterns like solitons or breathers, then the total population imbalance is superposition of incoherent Rabi oscillations with different amplitudes and frequencies. As the intra-component interaction energy exceeds some threshold, then Rabi oscillations corresponding to distinct localized patterns cease, that is, these patterns become immiscible solitons comprising only one component of the mixture. In this case one observes simultaneously spatial and internal self-trapping. It should be mentioned that formation of immiscible solitons is preceded by a short chaotic transient and can be regarded as some kind of self-organization.

In the case of the initial state without spatial modulation, Rabi oscillations corresponding to different lattice sites can be synchronized. If the intra-component interaction is weak, the synchronization is total and the condensate undergoes Rabi oscillations as a whole. In the case of moderate intra-component interactions, Rabi oscillations at different sites have different frequencies, therefore total synchronization is destroyed. However, there can arise spontaneous synchronization inside a large lattice domain. It is shown that synchronized oscillations correspond to the same limit cycle in phase space portraits corresponding to individual lattice sites. Number of synchronized states strongly oscillates with time due the presence of wave-like excitations inside the domain of synchronization. On average, this number grows with time due to condensate expansion along the lattice.

Detailed study of the particular phenomena described in this paper, like spontaneous synchronization or formation of immiscible solitons, will be the object of our future work. In addition, we intend to go beyond the approximations used in derivation of Eqs. (3) and verify the results obtained with more realistic approaches. Firstly, one should use continuous mean-field approximation corresponding to the coupled Gross-Pitaevskii equations (1). This allows one to estimate the role of the inter-band Landau-Zener tunneling which is ignored in the tight-binding approximation. Another important advantage of the continuous mean-field approximation is the ability to avoid limitations on the nonlinearity coefficients g_1 ,

g_2 and g_{12} . These limitations are required for validity of the tight-binding approximation and discussed in Section 2.1.

Acknowledgments

The authors acknowledge the financial support provided within the RFBR project 12-02-31416, and the joint project of the Siberian and Far-Eastern Branches of the Russian Academy of Sciences (project 12-II-SO-07-022).

References

- [1] S. Raghavan, A. Smerzi, S. Fantoni, and S.R. Shenoy, *Phys. Rev. A*, **59**, 620 (1999).
- [2] T. Zibold, E. Nicklas, C. Gross, and M.K. Oberthaler, *Phys. Rev. Lett.*, **105**, 204101 (2010).
- [3] I.M. Merhasin, B.A. Malomed, and R. Driben, *J. Phys. B: At. Mol. Opt. Phys.*, **38**, 877 (2005).
- [4] E. Nicklas, H. Strobel, T. Zibold, C. Gross, B.A. Malomed, P.G. Kevrekidis, and M.K. Oberthaler, *Phys. Rev. Lett.*, **107**, 193001 (2011).
- [5] R. Gati, M.K. Oberthaler, *J. Phys. B: At. Mol. Opt. Phys.*, **40**, R61 (2007).
- [6] T. Byrnes, K. Wen, and Y. Yamamoto, *Phys. Rev. A*, **85**, 040306(R) (2012).
- [7] G. Kleine Büning, J. Will, W. Ertmer et al, *Phys. Rev. Lett.*, **106**, 240801 (2011).
- [8] F.S Cataliotti, S. Burger, C. Fort, P. Maddaloni, F. Minardi, A. Trombettoni, A. Smerzi, and M. Inguscio, *Science*, **293**, 843 (2001).
- [9] T. Calarco, U. Dorner, P. S. Julienne, C. J. Williams, and P. Zoller, *Phys. Rev. A*, **70**, 012306 (2004).
- [10] I. Bloch, *Nature*, **453**, 1016 (2008).
- [11] S.V. Prants and V.Yu. Sirotkin, *Phys. Rev. A*, **64**, 033412 (2001).
- [12] V. Yu. Argonov and S. V. Prants, *JETP*, **96**, 832 (2003) [*ZhETF*, **123**, 946 (2003)].
- [13] S. V. Prants and M. Yu. Uleysky, *Phys. Lett. A*, **309**, 357 (2003).
- [14] S.V. Prants, M.Yu. Uleysky, and V.Yu. Argonov, *Phys. Rev. A*, **73**, 023807 (2006).
- [15] V. Yu. Argonov and S. V. Prants, *Phys. Rev. A*, **75**, 063428 (2007).
- [16] S.V. Prants, *JETP Letters*, **75**, 651 (2002) [*Pis'ma ZhETF*, **75**, 777 (2002)].
- [17] S. V. Prants, M. Edelman, and G. M. Zaslavsky, *Phys. Rev. E*, **66**, 046222 (2002).
- [18] V. Yu. Argonov and S. V. Prants, *J. Russ. Laser Res.*, **27**, 360 (2006).
- [19] V. Yu. Argonov and S. V. Prants, *Phys. Rev. A*, **71**, 053408 (2005).

- [20] V. Yu. Argonov and S. V. Prants, *Phys. Rev. A*, **78**, 043413 (2008).
- [21] V.Yu. Argonov and S.V. Prants, *Europhys. Lett.*, **81**, 24003 (2008).
- [22] A. Trombettoni and A. Smerzi, *Phys. Rev. Lett.*, **86**, 2353 (2001).
- [23] Th. Anker, M. Albiez, R. Gati, S. Hunsmann, B. Elermann, A. Trombettoni, and M.K. Oberthaler, *Phys. Rev. Lett.*, **94**, 020403 (2005).
- [24] J. Ruostekoski, Z. Dutton, *Phys. Rev. A*, **76**, 063607 (2007).
- [25] A.R. Kolovsky and H.-J. Korsch, *J. Sib. Fed. Univ. Math. & Phys.*, **3**, 311 (2010).
- [26] D.N. Maksimov, I.Yu. Chesnokov, D.V. Makarov, and A.R. Kolovsky *J. Phys. B: At. Mol. Opt. Phys.*, **46**, 145302 (2013).
- [27] S. Ronen, J.L. Bohn, L.E. Halmø, and M. Edwards, *Phys. Rev. A*, **78**, 053613 (2008).
- [28] U. Shrestha and J. Ruostekoski, *New J. Phys.*, **14**, 043037 (2012).
- [29] J.C. Eilbeck, P.S. Lomdahl, and A.C. Scott, *Physica D*, **16**, 318 (1985).
- [30] G. Mazzaella, B. Malomed, L. Salasnich, M. Salerno, and F. Toigo, *J. Phys. B: At. Mol. Opt. Phys.*, **44**, 035301 (2011).
- [31] D.N. Maksimov, A.F. Sadreev, *Phys. Rev. E*, **88**, 032901 (2013).
- [32] R. Franzosi, R. Livi, G.-L. Oppo, and A. Politi, *Nonlinearity*, **24**, R89 (2011).
- [33] A.J. Leggett, *Rev. Mod. Phys.*, **73**, 307 (2001).
- [34] S.V. Prants, *JETP* **109**, 751 (2009) [*ZhETF* **136**, 872 (2009)].

